

Article

# Experimental Investigation of Chloride Uptake Performances of Hydrocalumite-Like Ca-Al LDHs with Different Microstructures

Shupeng Zhang<sup>1</sup>, Feng Yu<sup>1</sup>, Wenting He<sup>1</sup>, Dapeng Zheng<sup>1,2</sup>, Hongzhi Cui<sup>1,\*</sup>, Leyang Lv<sup>1,\*</sup>, Waiching Tang<sup>3</sup>  and Ningxu Han<sup>1</sup>

<sup>1</sup> College of Civil and Transportation Engineering, Shenzhen University, Shenzhen 518060, China; 815806703@njtech.edu.cn (S.Z.); yufeng2017@email.szu.edu.cn (F.Y.); 2016090186@email.szu.edu.cn (W.H.); dpzheng2-c@my.cityu.edu.hk (D.Z.); nxhan@szu.edu.cn (N.H.)

<sup>2</sup> Department of Architecture and Civil Engineering, City University of Hong Kong, Kowloon 999077, Hong Kong

<sup>3</sup> School of Architecture and Built Environment, The University of Newcastle, Callaghan, NSW 2308, Australia; patrick.tang@newcastle.edu.au

\* Correspondence: h.z.cui@szu.edu.cn (H.C.); l.lv@szu.edu.cn (L.L.); Tel.: +86-755-26917849 (H.C. & L.L.)

Received: 12 May 2020; Accepted: 26 May 2020; Published: 28 May 2020



**Abstract:** In this study, hydrocalumite-like  $\text{Ca}_2\text{Al-NO}_3^-$  layered double hydroxides (Ca-Al LDHs) with different microstructures were synthesized. The crystalline properties, structure composition, morphology and particle size distribution of the Ca-Al LDH (CAL) samples were illustrated. To obtain the chloride uptake performances of CAL, the influences of contact time, initial concentration of  $\text{Cl}^-$ , pH of reaction solution and coexistence anions on the chloride uptake were examined systematically. Compared to the CAL samples obtained at a higher aging temperature, CAL synthesized at  $60^\circ\text{C}$  demonstrated the minimum average particle size ( $6.148\ \mu\text{m}$ ) and the best  $\text{Cl}^-$  adsorption capacity ( $211.324\ \text{mg/g}$ ). Based on the test results, the main adsorption mechanism of chloride ion on CAL was recognized as an interlayer anion exchanging reaction other than the dissolution-precipitate mode. With the increase in the pH value of reaction solution from 7 to 13, it was found that the amount of chloride ion adsorbed by CAL increased slightly, and the solution could remain at relatively high pH value even after the adsorption. The presence of  $\text{CO}_3^{2-}$  and  $\text{SO}_4^{2-}$  reduced the adsorption capacity of CAL dramatically as compared with  $\text{OH}^-$  due to the destruction of layered structure and the formation of precipitates ( $\text{CaCO}_3$  or  $\text{CaSO}_4$ ). The interference sequence of the investigated anions on the chloride uptake of CAL was  $\text{SO}_4^{2-}$ ,  $\text{CO}_3^{2-}$  and  $\text{OH}^-$ , and the order of interlayer anionic affinity was  $\text{Cl}^- > \text{OH}^- > \text{NO}_3^-$ . The results illustrated that the synthesized CAL could be used as a promising chloride ion adsorbent for the corrosion inhibition of reinforcement embedded cement-based materials.

**Keywords:**  $\text{Ca}_2\text{Al-NO}_3^-$  LDHs; aging temperature; particle size; chloride uptake; adsorption capacity; kinetic model

## 1. Introduction

Coarse aggregates account for approximately 30% to 40% of the total mass of concrete [1]. Previous studies reported that construction wastes can be applied as recycled concrete aggregates (RCA) to replace natural aggregate in concrete [2–4]. However, due to the fact that concrete casted with RCA will increase its porosity, the resistance of concrete to chloride ions is reduced and their wide application in construction is restricted [5]. In the past, various technologies and methods were developed in an attempt to address the issues of RCA. Pre-treatment of RCA such as mechanical

polishing [6] and chemical surface modification [7] have been found to be effective to remove the cement paste attached to the natural aggregate and improve the quality of recycled aggregate concrete. However, the implementation of these methods may also come with new problems such as high CO<sub>2</sub> emission, and environmental and safety concerns. Applying nanomaterials as filler to improve the compactness of concrete is another way to enhance the chloride resistance of recycled aggregate concrete. Nanoparticles such as nanoSiO<sub>2</sub> [8,9], nano-modified fly ash [10], nano-Al<sub>2</sub>O<sub>3</sub> [11], graphene oxide [12] are effective in strengthening the mechanical properties and chloride binding capacity of blended cement pastes. A previous study shows that the porosity reduced by 11.8% when 2% nano-SiO<sub>2</sub> was applied and the chloride resistance also showed an obvious improvement [13].

Layered double hydroxides (LDHs) are a novel layered dimensional nanomaterial, which has a sandwich-like multilayer structure. One of the significant advantages of LDHs is that the nanoparticles can reduce the porosity while improving the chloride binding capacity of recycled aggregate concrete [14,15]. Based on the brucite-like structure of LDH ( $[M_{1-x}^{2+}M_x^{3+}(\text{OH})_2]^{x+}$ ), some trivalent metal cations ( $M^{3+}$ ) can be isomorphous substituted by divalent metal cations ( $M^{2+}$ ), which will form positively charged LDH layers compensated by some interlayer anions ( $A^{n-}$ ). These interlayer anions bind to the main layer structure through weak hydrogen bonds or electrostatic interaction. Hence, some guest anions in the surrounding environment will easily exchange the initial interlayer anion and thus intercalate into the layered structure. This anion exchangeability enables LDHs to be used as a vital adsorbent in chemical engineering. Hydrocalumite ( $\text{Ca}_2\text{Al}(\text{OH})_6\text{Cl}\cdot 2\text{H}_2\text{O}$ , CAL) is one of typical natural LDHs, which has been applied to improve the durability of cementitious materials due to its excellent anion exchange or adsorption property. Chi et al. reported that the CAL precursor prepared by the optimized synthesis method could effectively immobilize chloride from sodium chloride solution and it is a potential adsorbent to protect the reinforced concrete from chlorine corrosion [16]. Chen et al. indicated that the free chloride ion in the pore solution could be effectively immobilized by CAL through an anion exchange mechanism [17]. Chung et al. found that the compressive strength of cement mortar samples will not be significantly affected when the amount of CAL replacement for cement does not exceed 10% [18]. More recently, nano CAL with different particle sizes were prepared by varying pH value [19]. It was found that the particle size of CAL plays significant roles in the microstructure and permeability improvement of cement paste. CAL with a smaller particle size has better chloride binding and physical barrier effect than the larger ones. So, the mortars containing smaller CAL can reduce the chloride migration coefficient better.

In this study, nano CALs with different microstructures were prepared by accurately controlling the aging temperature during the preparation. Compared with other research methods, such as controlling the pH of the reaction solution, the proposed temperature controlling method is more accurate and convenient, which offers great potential for the application of LDH in actual engineering. To investigate the working mechanism of CAL in chlorine adsorption, characterization methods including X-ray diffraction (XRD), Fourier transform infrared spectra (FT-IR), scanning electron microscope (SEM) and dynamic laser scattering (DLS) instruments were used to illustrate the crystalline properties, structure composition, morphology and particle size distribution of the CAL, respectively. The influences of contact time, initial concentration of Cl<sup>-</sup>, pH of reaction solution and coexistence anions on the chloride uptake of CAL were also examined. The results from this study can fill the knowledge gap about chloride uptake performances of CALs with different microstructures under the simulation of concrete eroded by CO<sub>2</sub> and Cl<sup>-</sup>.

## 2. Materials and Methods

### 2.1. Materials

Calcium nitrate tetrahydrate, aluminum nitrate nonahydrate, sodium hydroxide, sodium chloride and sodium sulfate anhydrous were supplied by Guangdong Guanghua Sci-Tech. Co., Ltd. Sodium carbonate anhydrous (Na<sub>2</sub>CO<sub>3</sub>) was obtained from Xilong Scientific Co., Ltd. (Guangdong, China).

Deionized water was used for all experiment processes, including CAL synthesis and solution preparation. All the reagents used in this work were of analytical grade.

### 2.2. Synthesis of Hydrocalumite-Like CaAl-NO<sub>3</sub>- LDHs

The co-precipitation technique combined with aging steps method was applied to synthesize CAL. First, 23.62 g (0.1 mol) of calcium nitrate tetrahydrate and 18.76 g (0.05 mol) of aluminum nitrate nonahydrate were dissolved in 70 mL of deionized water to obtain metal salt precursor solution A, and 150 mL of NaOH solution with 2 M concentration was prepared as alkaline solution B. Under a vigorous stirring (2500 rpm) at room temperature (25 °C), the metal salt solution A was added dropwise into the alkaline solution B within an hour to keep the pH values at around 10.8–11. After 30 min of stirring, the resulting precipitate was collected by centrifugation and rinsed with the deionized water twice. Then the obtained product was added with 220 mL of deionized water again and dispersed by means of ultra-sonication. After the dispersion, the mixture was poured into a 300 mL Teflon autoclave reactor and heated at various temperature levels (60–120 °C) for 12 h. Finally, the resulting suspension was dried in a freeze dryer until the formation of a powder-like dry CAL.

### 2.3. Characterization

X-ray diffraction (XRD) patterns of LDHs ( $2\theta = 3^\circ\text{--}70^\circ$ ) were recorded by using a Bruker D8 Advance X-ray diffractometer, and the scanning rate was set as  $2^\circ/\text{min}$ . Fourier transform infrared spectra (FT-IR) testing of CAL powder was recorded from 400 to 4000  $\text{cm}^{-1}$  by applying a Nicolet 6700 FTIR spectrometer. Microstructure characteristics of CAL samples were examined by adopting a Phenom Pro (Phenom-World, USA) scanning electron microscope (SEM). Wide-angle dynamic laser scattering (DLS) instrument (Mastersizer 2000, Malvern Panalytical, Malvern, UK) was applied to measure the particle size distribution of CAL samples prepared with different aging temperatures.

### 2.4. Adsorption Studies

Before the adsorption experiments, chloride solution with a series of concentrations of 1–240 mmol/L was achieved using a continuous dilution method. To study the influence of chloride concentration on the  $\text{Cl}^-$  uptake of CAL, 1 g of each CAL samples was added into some conical flasks containing 100 mL sodium chloride solution with various  $\text{Cl}^-$  concentrations. After sealing these conical flasks, the mixture was magnetically stirred vigorously for 24 h at 25 °C. The supernatant in the conical flasks was obtained by centrifugation for the determination of  $\text{Cl}^-$  concentration. The amount of  $\text{Cl}^-$  adsorbed by CAL was determined by potentiometric titration and calculated by the following formula:

$$Q_e = \frac{V \times (C_0 - C_e) \times 35.45}{m} \quad (1)$$

where  $Q_e$  ( $\text{mg}\cdot\text{g}^{-1}$ ) is the adsorbance of  $\text{Cl}^-$  by CAL,  $V$  (L) represents the volume of NaCl solution,  $C_0$  and  $C_e$  ( $\text{mmol}\cdot\text{L}^{-1}$ ) are the initial and equilibrium concentration of  $\text{Cl}^-$ , respectively. The number 35.45 is the relative molecular mass of chloride ion and  $m$  (g) is the mass of CAL.

To examine the effect of reaction time on the adsorbance of  $\text{Cl}^-$  by CAL, i.e., adsorption kinetics, CAL sample was added into the conical flasks containing 100 mL sodium chloride solution and stirred vigorously for different specified times. Then the supernatant in the conical flask was centrifuged at a predetermined time and the concentration of  $\text{Cl}^-$  was determined.

To simulate the pH conditions of carbonated and uncarbonated cement pore solutions, NaOH solution with 0.1 M concentration was chosen to adjust the initial pH values of NaCl solution as 7–13. The initial concentration of  $\text{Cl}^-$  solution and reaction time was fixed as 80 mmol/L and 2, respectively. In addition, the other experimental conditions were kept the same as above. The effect of coexistence anions (such as  $\text{OH}^-$ ,  $\text{SO}_4^{2-}$  and  $\text{CO}_3^{2-}$ ) on  $\text{Cl}^-$  uptake of CAL was also studied. The initial concentrations of those interfering anions were set as 40 mmol/L and 80 mmol/L while the other

experimental conditions including contact time, temperature and initial  $\text{Cl}^-$  concentration were also fixed as described above.

### 3. Results and Discussion

#### 3.1. Characterization of CAL

To investigate the influence of aging temperature on the crystallizing behaviors of as-synthesized CAL, XRD patterns were obtained as shown in Figure 1. XRD patterns (a) and FT-IR spectra (b) of  $\text{CaAl-NO}_3^-$  layered double hydroxides (LDHs) prepared at different temperatures (samples were indicated as CAL-x, where x = aging temperature, 60–120 °C) are shown in Figure 1. It was found that no calcium carbonate byproduct formed in the CAL samples synthesized at 60–120 °C. The CAL samples collected at different temperatures exhibited multiple diffraction peaks at 10.3°, 20.6°, 31.3°, 37.6°, 44.5° and 46.0° (2 $\theta$ ), which was consistent with those reported using the similar method [20]. These peaks correspond to (002), (004), (110), (114), (116) and (018) diffraction planes of the typical CAL structure with nitrate anion intercalated between the main layer (PDF-#54-0849). By comparing (002) and (004) diffraction peak intensities of different samples, it was found that the crystallinity of CAL increased with elevating aging temperature, and the similar results were also reported by Xu [21]. Moreover, the basic layer spacing (distance between two layers + one single layer) can be calculated at (002) diffraction peak by using the Bragg equation. In general, variation of the basic layer spacing at the first diffraction peak indicates clearly that LDHs are completely or partially intercalated by guest anions [22]. All the CAL samples showed the similar spacing  $d_{002}$  values ranged from 0.858 to 0.876 nm, which was in good agreement with the previously reported values [23,24].

The FT-IR spectra of CAL samples (see Figure 1. XRD patterns (a) and FT-IR spectra (b) of  $\text{CaAl-NO}_3^-$  layered double hydroxides (LDHs) prepared at different temperatures (samples were indicated as CAL-x, where x = aging temperature, 60–120 °C) are shown in Figure 1. b) exhibited similar vibration characteristics of LDHs structure, and the aging temperature had little effect on their structure. Broad bands observed at 3636  $\text{cm}^{-1}$  and 3472  $\text{cm}^{-1}$  in all CAL were ascribed to the stretching vibration of hydroxyl existed in the hydroxide layer structure, interlayer water and adsorbed water molecules of CAL [25,26], while the bending vibration of H-O-H existed in some water molecule was observed at 1638  $\text{cm}^{-1}$  [27]. The overlapping peaks showed at 1300–1500  $\text{cm}^{-1}$  were ascribed to the antisymmetric stretching vibration of  $\text{CO}_3^{2-}$  (1430  $\text{cm}^{-1}$ ) [26–28] and interlayer nitrate groups of  $\text{CaAl-NO}_3^-$  LDHs (1353  $\text{cm}^{-1}$ ) [23], indicating that the as-synthesized CAL samples might be carbonated during their preparation due to  $\text{CO}_2$  in the atmosphere. It should be noted that no obvious diffraction peaks of carbonates (e.g., calcite) can be observed in the XRD patterns (Figure 1. XRD patterns (a) and FT-IR spectra (b) of  $\text{CaAl-NO}_3^-$  layered double hydroxides (LDHs) prepared at different temperatures (samples were indicated as CAL-x, where x = aging temperature, 60–120 °C) are shown in Figure 1. a), which may be related to the stronger diffraction peak of  $\text{CaAl-NO}_3^-$  LDH phase. The other peaks at 500–800  $\text{cm}^{-1}$  were caused by the lattice vibrations of M-O or M-OH (M represents metal, e.g., Ca or Al).

SEM images showed the morphology of CAL samples synthesized at different aging temperatures (Figure 2. SEM images of  $\text{CaAl-NO}_3^-$  LDH samples synthesized at different temperatures ((a) 60 °C, (b) 70 °C, (c) 80 °C, (d) 100 °C, and (e) 120 °C)). It was found that all the CAL samples exhibited regular hexagonal flake-like particle morphology corresponding to hydrocalumite compounds. Overall, the enhancement of the particle size of CAL with increasing aging temperature can be clearly observed in Figure 2. SEM images of  $\text{CaAl-NO}_3^-$  LDH samples synthesized at different temperatures ((a) 60 °C, (b) 70 °C, (c) 80 °C, (d) 100 °C, and (e) 120 °C). As compared with the CAL sample synthesized at 60 °C, CAL-120 had a sharper particle edge and more regular morphology, indicating a higher crystallinity of CAL-120 compared to CAL-60. The CAL synthesized at 60 °C and 70 °C showed similar particle size and crystallinity, which was consistent with the intensity and sharpness of diffraction peaks increasing with the elevation of the aging temperature, as can be seen in Figure 1. XRD patterns (a) and FT-IR spectra (b) of  $\text{CaAl-NO}_3^-$  layered double hydroxides (LDHs) prepared at different temperatures (samples were indicated as CAL-x, where x = aging temperature, 60–120 °C). To further determine

the effect of aging temperature on particle size of CAL, particle size distribution of  $\text{CaAl-NO}_3^-$  LDHs prepared at various aging temperatures were given in Figure 3. Particle size distribution obtained by dynamic laser scattering (DLS) analysis of the Ca-Al LDH (CAL) samples prepared at different aging temperatures. The average particle size of CAL obtained at 60, 70, 80, 100 and 120 °C was 6.148, 11.580, 11.829, 14.278 and 22.932  $\mu\text{m}$ , respectively. This variation tendency of particle size was consistent with the above SEM images observation results.

The aging temperature has an important influence on the synthesis of LDHs, especially on the development of crystalline grains. Crystal growth, agglomeration or lamination occurred simultaneously in the heat treatment of CAL [29]. Metal hydroxide precursors formed at the initial stage of CAL synthesis can be used as seeds of CAL crystals. Increasing aging temperature can not only promote the formation of these seeds, but also increase the recombination rate of microcrystals in solution. Moreover, the crystal growing rule of CAL can be illustrated by Oswald's aging mechanism, that is, aging temperature enhancement will promote the dissolution of smaller particles and then promote the growth of particles with a larger size [29,30]. Subsequently, these particles were stacked continuously to form larger CAL particles with more stacked layers and larger lateral dimensions.

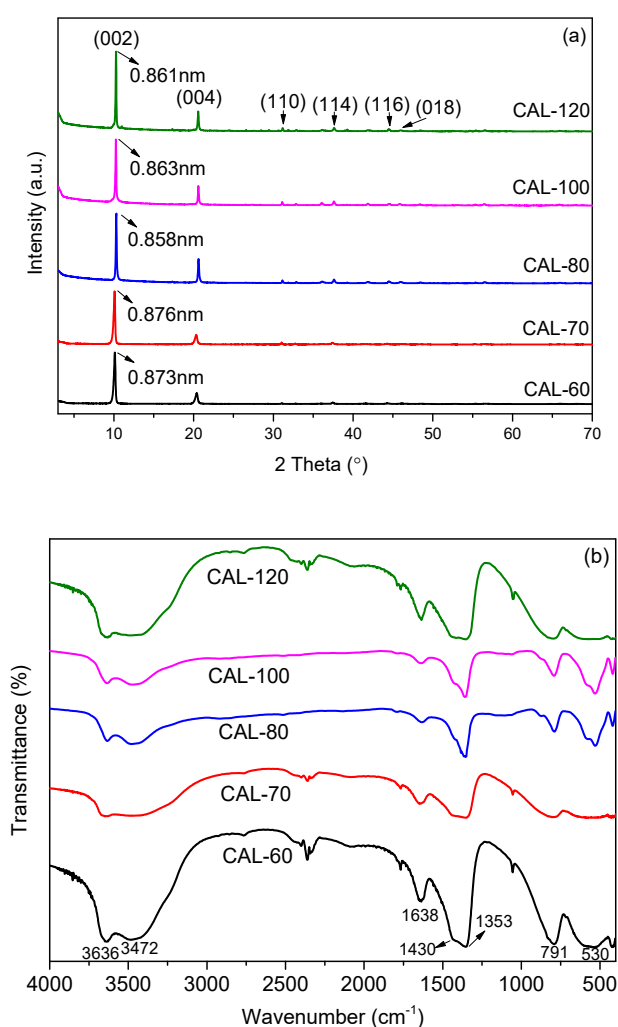


**Figure 1.** XRD patterns (a) and FT-IR spectra (b) of  $\text{CaAl-NO}_3^-$  layered double hydroxides (LDHs) prepared at different temperatures (samples were indicated as CAL-x, where x = aging temperature, 60–120 °C).

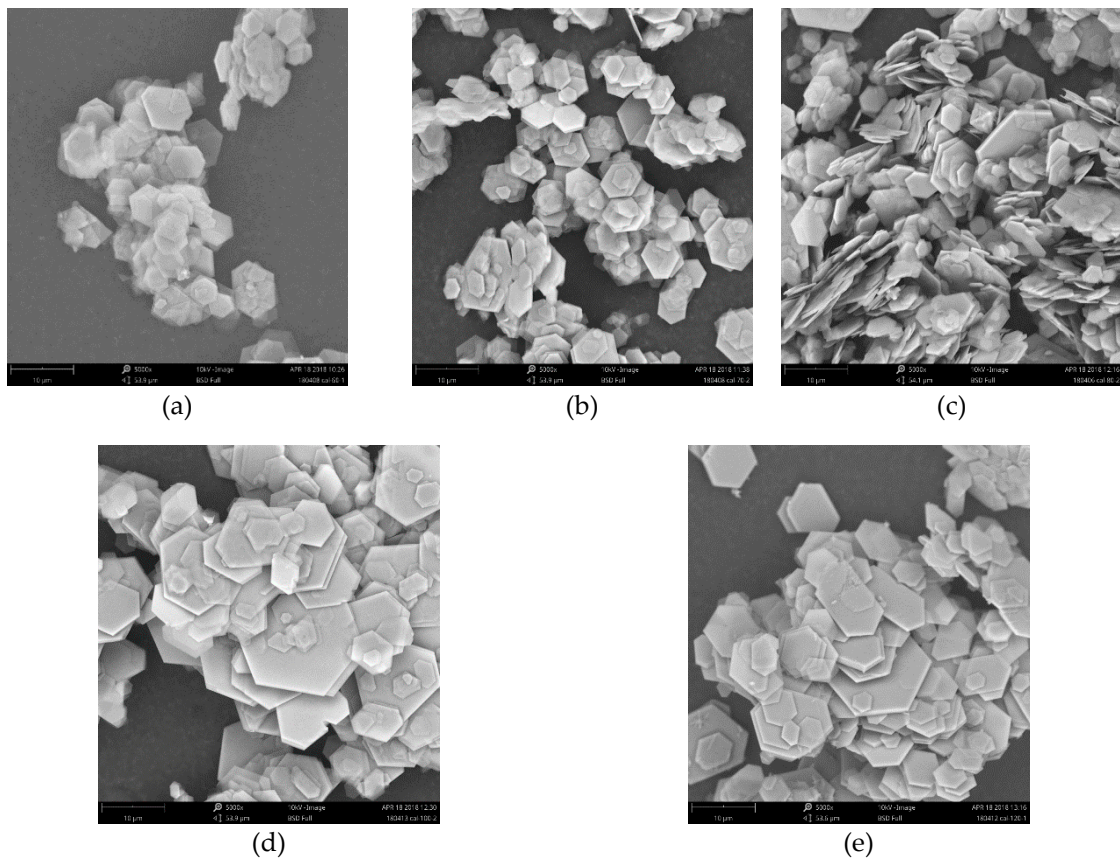


**Figure 2.** SEM images of  $\text{CaAl-NO}_3^-$  LDH samples synthesized at different temperatures ((a) 60 °C, (b) 70 °C, (c) 80 °C, (d) 100 °C, and (e) 120 °C).

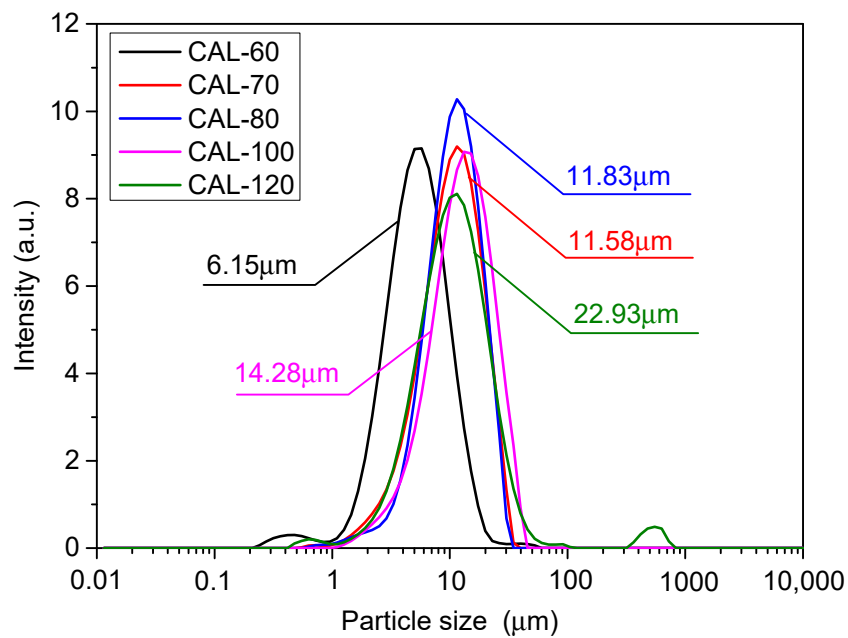


**Figure 3.** Particle size distribution obtained by dynamic laser scattering (DLS) analysis of the Ca-Al LDH (CAL) samples prepared at different aging temperatures.

### 3.2. Effect of Contact Time

The adsorption kinetics curve of chloride ion on the CAL-60 sample was shown in Figure 4. The influence of reaction time on the  $\text{Cl}^-$  uptake on CAL-60 and nonlinear fits achieved using Pseudo-first-order model and Pseudo-second-order model (Temperature = 25 °C; CAL sample/NaCl solution = 10 g/L; initial chloride ion concentration and pH was set as 80 mmol/L and 7, respectively). Two adsorption kinetics models (Pseudo-first-order and Pseudo-second-order model) were used to fit the experimental results as follows:

$$\ln(Q_e - Q_t) = \ln Q_e - k_1 t \quad (2)$$

$$\frac{t}{Q_t} = \frac{1}{k_2 Q_e^2} + \frac{t}{Q_e} \quad (3)$$

where  $Q_t$  ( $\text{mg}\cdot\text{g}^{-1}$ ) and  $Q_e$  ( $\text{mg}\cdot\text{g}^{-1}$ ) are the  $\text{Cl}^-$  uptake on CAL at  $t$  time and equilibrium, respectively;  $k_1$  and  $k_2$  are the kinetics correlation of Pseudo-first-order constant and rate correlation constant of Pseudo-second-order, respectively.

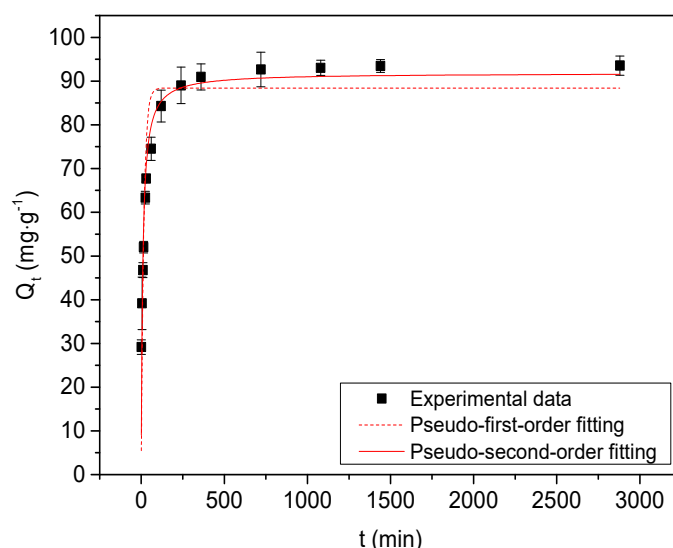


**Figure 4.** The influence of reaction time on the  $\text{Cl}^-$  uptake on CAL-60 and nonlinear fits achieved using Pseudo-first-order model and Pseudo-second-order model (Temperature = 25 °C; CAL sample/NaCl solution = 10 g/L; initial chloride ion concentration and pH was set as 80 mmol/L and 7, respectively).

It was observed that the absorbance of chloride ion by CAL rapidly increased at an initial 240 min, and then increased slowly at 500–3000 min reaching to equilibrium, with the maximum of 93.548 mg/g. This rapid adsorption (<240 min) involving LDHs was attributed with anion exchange reaction [31] ( $\text{NO}_3^-$  is replaced by  $\text{Cl}^-$ ) and the abundant adsorption sites of LDHs [32], while the adsorption capacity changed little with contact time during the equilibrium period (500–3000 min) due to the limited adsorption sites of LDHs.

Table 1 showed a series of kinetics parameters calculated by the above two adsorption kinetics models. By comparing the correlation coefficients ( $R^2$ ) of above two kinetics models, it can be seen that the Pseudo-second-order model with  $R^2$  of 0.948 described the experimental data of CAL-60 better, implying the occurrence of chemisorption, which was ascribed to a rate-limiting step [32,33]. The adsorption capacity of  $\text{Cl}^-$  on CAL-60 at equilibrium achieved by Pseudo-second-order kinetics model was 91.844  $\text{mg}\cdot\text{g}^{-1}$ , which was close to the experimental data (93.548  $\text{mg}\cdot\text{g}^{-1}$ ).

**Table 1.** Experimental data of Cl<sup>-</sup> uptake on CAL-60 and adsorption kinetics parameters obtained from two adsorption kinetics models.

Samples	Q <sub>e,ex</sub> (mg·g <sup>-1</sup> )	Pseudo-First-Order			Pseudo-Second-Order		
		Q <sub>e,ca</sub> (mg·g <sup>-1</sup> )	k <sub>1</sub> (1·min <sup>-1</sup> )	R <sup>2</sup>	Q <sub>e,ca</sub> (mg·g <sup>-1</sup> )	k <sub>1</sub> (g·mg <sup>-1</sup> ·min <sup>-1</sup> )	R <sup>2</sup>
CAL-60	93.548	88.417	0.064	0.906	91.844	0.00119	0.948

### 3.3. Effect of Initial Cl<sup>-</sup> Concentration

To examine the effect of initial Cl<sup>-</sup> concentration on the chloride ion removal by CAL, an adsorption isothermal experiment was conducted at room temperature (25 °C). Figure 5. The effect of initial Cl<sup>-</sup> concentration on Cl<sup>-</sup> adsorption on CAL and nonlinear fits achieved using Freundlich isotherm and Langmuir isotherm ((a) CAL-60; (b) CAL-70; (c) CAL-80; (d) CAL-100; (e) CAL-120) exhibits the adsorption isotherms of CAL. Langmuir and Freundlich equations were used for nonlinear fitting of data as expressed in the following:

$$Q_e = \frac{Q_m k_L C_e}{1 + k_L C_e} \tag{4}$$

$$Q_e = k_F C_e^{1/n} \tag{5}$$

where C<sub>e</sub> (mmol·L<sup>-1</sup>) and Q<sub>e</sub> (mg·g<sup>-1</sup>) are the equilibrium concentration of remain chloride and adsorption capacity of chloride ion by CAL at equilibrium, respectively. Q<sub>m</sub> (mg·g<sup>-1</sup>) represents the maximum adsorption amount of Cl<sup>-</sup> on CAL calculated by Langmuir isotherm, k<sub>L</sub> (L·mg<sup>-1</sup>) is Langmuir constant, which affects the adsorption ability and binding energy. k<sub>F</sub> ((mg/g) (L/mg)<sup>1/n</sup>) and 1/n are Freundlich constants, which affect the adsorption capacity and strength of adsorbent, respectively.

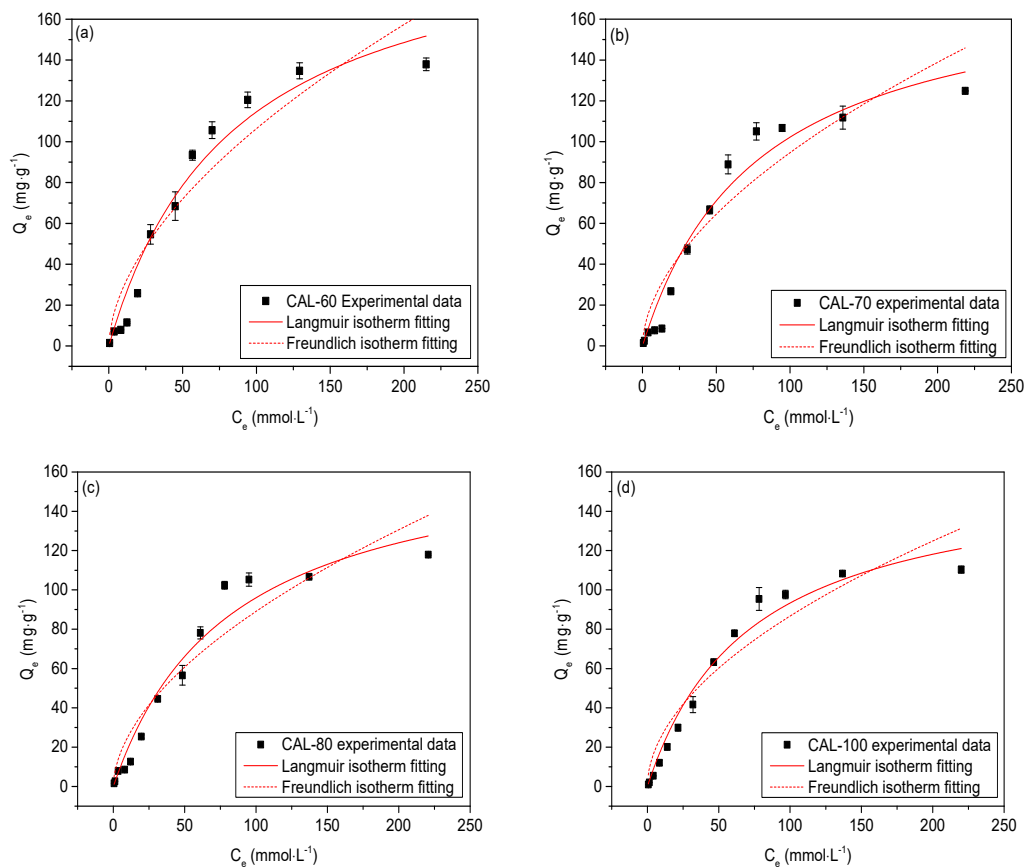


**Figure 5.** Cont.

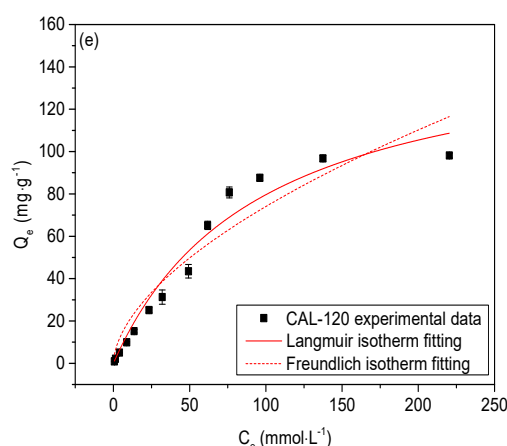


**Figure 5.** The effect of initial  $\text{Cl}^-$  concentration on  $\text{Cl}^-$  adsorption on CAL and nonlinear fits achieved using Freundlich isotherm and Langmuir isotherm ((a) CAL-60; (b) CAL-70; (c) CAL-80; (d) CAL-100; (e) CAL-120).

The fitting results using the above two isotherm models are exhibited in Figure 5. The effect of initial  $\text{Cl}^-$  concentration on  $\text{Cl}^-$  adsorption on CAL and nonlinear fits achieved using Freundlich isotherm and Langmuir isotherm ((a) CAL-60; (b) CAL-70; (c) CAL-80; (d) CAL-100; (e) CAL-120) and Table 2. Langmuir isotherm fitting showed a higher correlation coefficient ( $R^2$ ) as compared with Freundlich isotherm (Table 2), suggesting that the Langmuir isotherm was more consistent with the experimental results than the Freundlich isotherm. The  $1/n$  value of Freundlich isotherm ranged from 0 to 1 and suggested a favorable adsorption [33,34]. According to the results shown in Table 2, the  $1/n$  values for all CAL samples (0.526–0.574) indicated that the adsorption of  $\text{Cl}^-$  on synthesized CAL was favorable. The theoretical maximum absorbance of chloride ion by CAL samples calculated from Langmuir equation was 211.324 mg/g, 182.117 mg/g, 174.903 mg/g, 160.914 mg/g and 155.960 mg/g, respectively, suggesting that enhancing aging temperature can improve the maximum adsorption capacity. Similar to other LDH-like materials, the particle size of CAL exhibited a significant effect on the adsorption performance. On the one hand, the particle size reduction can increase the specific area of CAL, which will offer more adsorption sites for  $\text{Cl}^-$  resulting in a higher adsorption capacity [35]. Additionally, more coordination sites with less coordination number for anion exchange will be formed (like the edge area of LDHs) [29,36] due to the reduction of particle size, which can enhance the removal efficiency of CAL.

**Table 2.** Experimental data of  $\text{Cl}^-$  uptake on CAL samples at equilibrium and fitting parameters achieved from Langmuir isotherm and Freundlich isotherm.

Sample	$Q_{m,ex}$ ( $\text{mg}\cdot\text{g}^{-1}$ )	Langmuir Isotherm			Freundlich Isotherm		
		$Q_{m,ca}$ ( $\text{mg}\cdot\text{g}^{-1}$ )	$k_L$ ( $\text{L}\cdot\text{mg}^{-1}$ )	$R^2$	$k_F$ ( $\text{mg}\cdot\text{g}^{-1}$ ) ( $\text{L}\cdot\text{mg}^{-1}$ ) $^{1/n}$	$1/n$	$R^2$
CAL-60	137.929	211.324	0.01185	0.972	7.89054	0.56491	0.922
CAL-70	124.890	182.117	0.01279	0.968	7.40587	0.55328	0.913
CAL-80	117.921	174.903	0.01217	0.970	7.01206	0.55201	0.921
CAL-100	110.340	160.914	0.01381	0.977	7.68250	0.52628	0.920
CAL-120	98.144	155.960	0.01043	0.967	5.27952	0.57350	0.925

### 3.4. Effect of Initial pH

To simulated the uptake of  $\text{Cl}^-$  in the pore solution of normal or carbonated cement-based materials (pH = 7–13.5), chloride uptake of CAL-60 at different pH conditions was conducted, as shown in Figure 6. Chloride uptake of CAL-60 in NaCl solution with different pH. The adsorption of  $\text{Cl}^-$  on CAL-60 at pH = 7, 8, 10, 12 and 13 were 95.5 mg/g, 99.7 mg/g, 100.4 mg/g, 102.5 mg/g and 106.0 mg/g,

respectively. It seems that the adsorption capacity of CAL-60 increased slightly with the enhancement of pH value. Moreover, the final pH of the mixture at equilibrium was almost in a stable range (pH = 11–12), which was favorable to maintain the alkaline environment of cement-based materials.

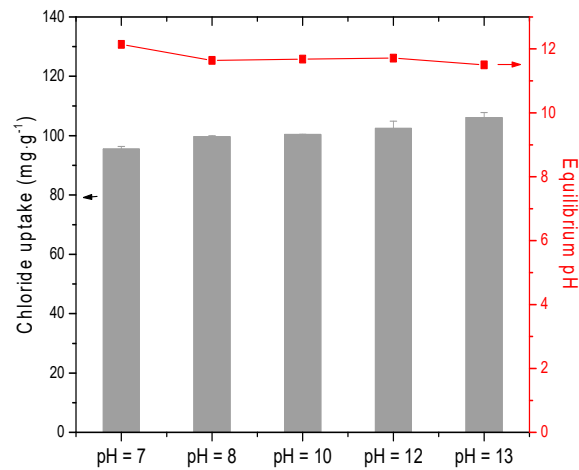


**Figure 6.** Chloride uptake of CAL-60 in NaCl solution with different pH (temperature = 25 °C; CAL/NaCl solution = 10 g/L; initial chloride ion concentration was set as 80 mmol/L).

Figure 7. XRD patterns of CAL-60 and CAL-60 samples after adsorption of Cl<sup>-</sup> under different pH conditions (N refers for CaAl-NO<sub>3</sub><sup>-</sup> type LDH; H refers for Hydrocalumite) shows the XRD results of CAL-60 and CAL-60 samples after adsorption of Cl<sup>-</sup> under different pH conditions. Compared with the pristine phase of CAL-60, hydrocalumite (Ca<sub>2</sub>Al(OH)<sub>6</sub>Cl·2H<sub>2</sub>O, PDF#31-0245) was indexed in the samples collected after adsorption of Cl<sup>-</sup> with different pH values. The d<sub>002</sub> value was varied accordingly from 0.87 to 0.79 nm correspondingly, which was related to the change of interlayer anions of CAL. As previously reported, hydrocalumite-like LDHs had a higher solubility than hydrotalcite-like LDHs [37]. During the adsorption of Cl<sup>-</sup> on CAL (Equation (6)), the calcium metal ion, soluble aluminum (Al(OH)<sub>4</sub><sup>-</sup> [37,38] and hydroxyl ion released due to the incomplete dissolution of CAL by the following reaction (Equation (7)), and the dissolution was faster at lower initial pH of solution, which will increase the pH value of solution as shown in Figure 6. But OH<sup>-</sup> will compete with Cl<sup>-</sup> adsorption at higher initial pH [39] (Equation (8)), resulting in a decrease in the pH of the solution.



Therefore, the adsorption of some inorganic anions on hydrocalumite-like LDHs was a dissolution–precipitation process. Qian et al. [38] found that the removal mechanism of phosphate by hydrocalumite involved the free calcium and aluminum ions released due to dissolution and then precipitated with phosphate to form hydroxyapatite. However, the exchange reaction of interlay anions was the main adsorption mechanism of chromate on hydrocalumite. In this work, the phase variation of the products was not pH-dependent and no calcium hydroxide phase observed in the XRD patterns (Figure 7) indicating that the removal of chloride ion was the result of anion exchange reaction between NO<sub>3</sub><sup>-</sup> and Cl<sup>-</sup> rather than the precipitation of chloride ion with calcium ion released by the dissolution of CAL. Moreover, the enhancement of chloride uptake with increasing pH value may be related to the inhibition of CAL dissolution at a higher pH [38].

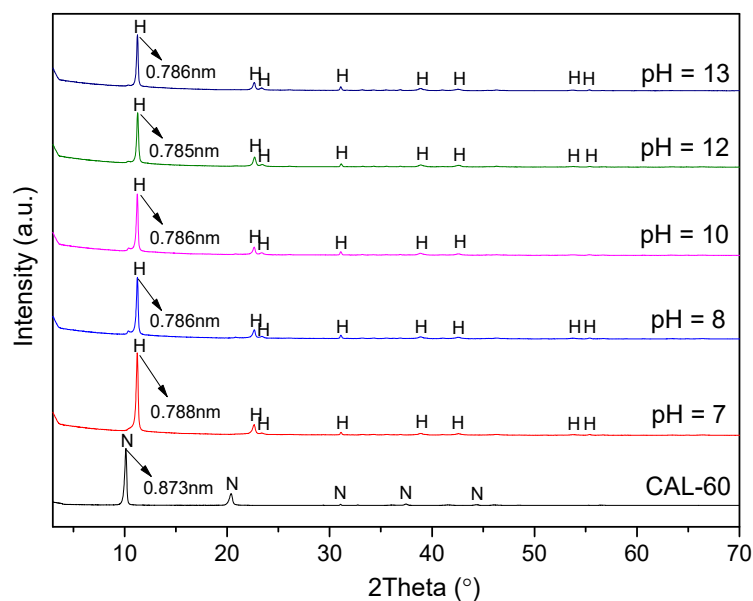


**Figure 7.** XRD patterns of CAL-60 and CAL-60 samples after adsorption of  $\text{Cl}^-$  under different pH conditions (N refers for  $\text{CaAl-NO}_3^-$  type LDH; H refers for Hydrocalumite).

### 3.5. Effect of Coexistence Anions and Adsorptive Selectivity of CAL

In general, there are some anions such as  $\text{OH}^-$ ,  $\text{SO}_4^{2-}$  and  $\text{CO}_3^{2-}$  existing simultaneously in the pore solution of cement-based materials, which might hinder the removal of chloride ions by the synthesized CAL adsorbents. Therefore, the influence of foreign anions on the chloride uptake of CAL sample was investigated in which the initial concentration of  $\text{Cl}^-$  was 80 mmol/L, the concentration of coexistence anions was kept at 40 mmol/L and 80 mmol/L and the other parameters remained unchanged. As shown in Figure 8, the removal efficiency of  $\text{Cl}^-$  by CAL-60 decreased with increasing the concentration of coexistence anions. For hydroxyl ions, CAL-60 performed a slight enhancement in the adsorption of chloride ion at 40 mmol/L of  $\text{OH}^-$ , which may be due to the inhibition of CAL dissolution by high alkalinity as described above. While the concentration of  $\text{OH}^-$  was increased to 80 mmol/L, the chloride uptake reduced, which was related to the excessive  $\text{OH}^-$  and  $\text{Cl}^-$  competing for the interlayer adsorption sites of CAL. For the oxyanion such as  $\text{CO}_3^{2-}$  and  $\text{SO}_4^{2-}$ , their presence can significantly reduce the chloride ion removal efficiency of CAL-60. When their concentration was 80 mmol/L,  $\text{Cl}^-$  uptake of CAL-60 showed a significant reduction from  $95.5 \text{ mg}\cdot\text{g}^{-1}$  to  $0.89 \text{ mg}\cdot\text{g}^{-1}$  and  $1.59 \text{ mg}\cdot\text{g}^{-1}$ , respectively. Meanwhile, when the three anions appeared in the adsorption system simultaneously, the high concentration of co-existing anions also significantly reduced the removal rate of CAL-60.

To evaluate the interaction mechanism of CAL-60 and  $\text{Cl}^-$  in the solution containing different interference anions, XRD was used to characterize the composition of samples collected before and after the chloride adsorption of CAL-60. As shown in Figure 9, it was observed that three coexistence anions had different effects on the phase change of CAL-60. In the presence of hydroxyl ions (40 mmol/L or 80 mmol/L), CAL-60 performed a phase transformation from  $\text{CaAl-NO}_3^-$  LDHs to  $\text{CaAl-Cl}^-$  LDHs (hydrocalumite phase) and a reduction of  $d_{002}$  value from 0.873 to 0.786 nm (see Figure 9a), indicating that the adsorption of  $\text{Cl}^-$  on CAL occurred through anion exchange reaction between  $\text{NO}_3^-$  and  $\text{Cl}^-$ . In contrast, the characteristic diffraction peaks of CAL utterly disappeared after 24 h of mixing with a solution containing  $\text{Cl}^-$  and  $\text{SO}_4^{2-}$ . Meanwhile, there were only some calcium sulfate and sodium chloride residues with poor crystallinity in the samples collected after mixing (see Figure 9b). This could suggest that the layered structure of CAL-60 was completely destroyed due to its dissolution. Consequently,  $\text{Cl}^-$  cannot be adsorbed by CAL through anion exchange reactions, while calcium sulfate is formed by the precipitation between  $\text{Ca}^{2+}$  released by CAL and  $\text{SO}_4^{2-}$ . Due to the above reasons, the

CAL sample completely lost its chlorine adsorption ability at higher concentrations of  $\text{SO}_4^{2-}$ , which was consistent with those results shown in Figure 8.

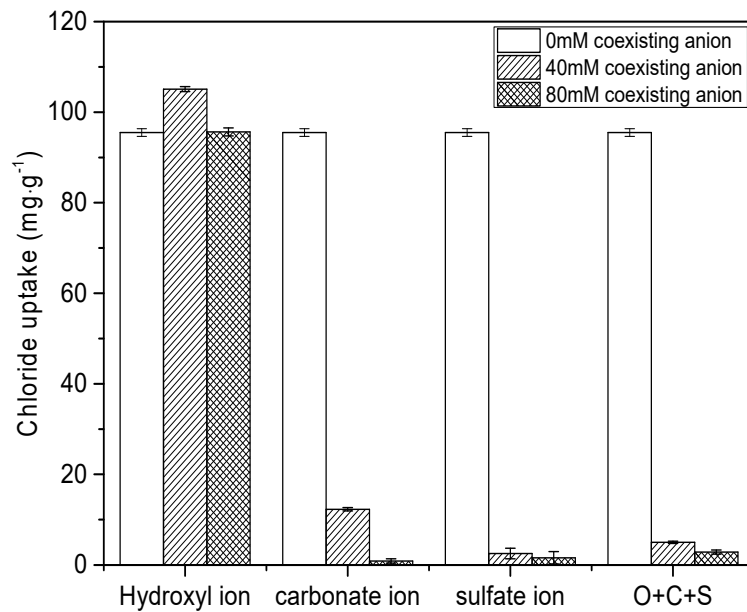


**Figure 8.** Effect of interference anions (i.e.,  $\text{OH}^-$ ,  $\text{CO}_3^{2-}$  and  $\text{SO}_4^{2-}$ ) on chloride uptake of CAL-60 (temperature = 25 °C; CAL/NaCl solution = 10 g/L; initial chloride ion concentration and pH was set as 80 mmol/L and 7, respectively).

Moreover, the carbonate ions with higher concentration also deposited with free calcium ions to form calcium carbonate precipitate, and finally completely destroyed the layered structure of CAL (see Figure 9c,d), which was similar to  $\text{SO}_4^{2-}$ . However, when the concentration of  $\text{CO}_3^{2-}$  was 40 mmol/L, CAL-60 sample retained the layered structure to adsorb  $\text{Cl}^-$  by anion exchange ( $d_{002}$  from 0.873 to 0.783 nm) due to its incomplete dissolution. Those small amounts of calcium carbonate covered the surface of CAL-60 which hindered its chloride adsorption. As shown in Figure 9d, the phase change of CAL before and after chloride uptake was similar to that case in solution containing  $\text{CO}_3^{2-}$ . Therefore, it can be deduced that interference sequence of three anions on the chloride uptake of CAL-60 was  $\text{SO}_4^{2-} > \text{CO}_3^{2-} > \text{OH}^-$ , and the order of interlayer anionic affinity was  $\text{Cl}^- > \text{OH}^- > \text{NO}_3^-$ , which was consistent with those results obtained by Chen et al. [17].

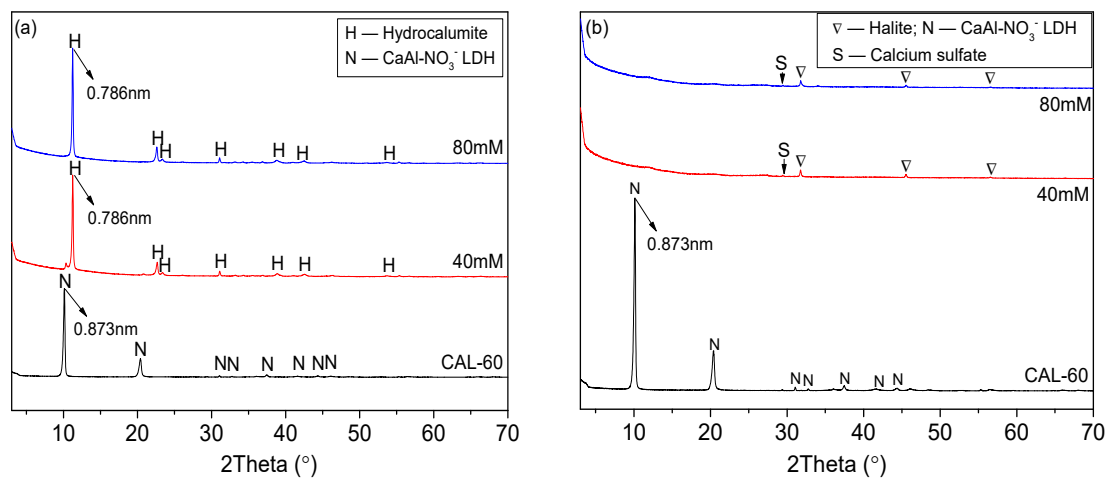


**Figure 9.** Cont.

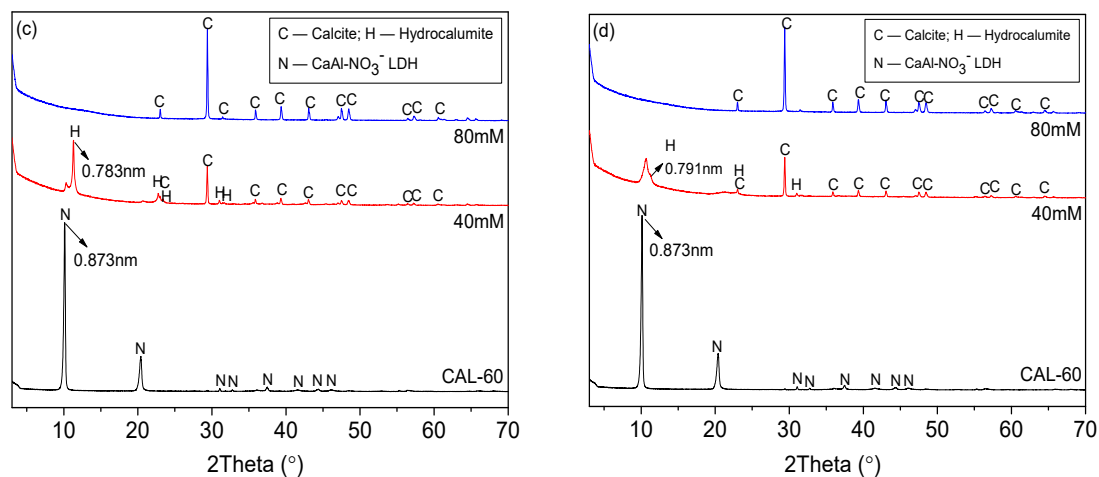


**Figure 9.** XRD patterns of solid phases after reaction by CAL-60 sample and 80 mM NaCl solution with different interference anions ((a)  $\text{OH}^-$ ; (b)  $\text{SO}_4^{2-}$ ; (c)  $\text{CO}_3^{2-}$ ; (d)  $\text{OH}^-$  and  $\text{SO}_4^{2-}$  and  $\text{CO}_3^{2-}$ ).

#### 4. Conclusions

Hydrocalumite-like  $\text{Ca}_2\text{Al-NO}_3^-$  LDH was synthesized based on a co-precipitation technique combined with an aging steps method. XRD, FT-IR, DLS, and SEM were used to characterize the crystalline properties, structure composition, particle size distribution, and morphology of CAL samples. The influences of contact time, initial concentration of  $\text{Cl}^-$ , pH of solution, and coexistence anions on the chloride uptake of CAL were also investigated. Based on the experimental results, some conclusions can be drawn as follows:

- (1) CAL samples synthesized at 60–120 °C performed a typical double hydroxide structure and the crystallinity of CAL increased slightly with increasing the aging temperature, which can be observed from XRD patterns. Enhancement of aging temperature also results in a sharper edge and larger particle size of CAL. The average particle size of CAL samples synthesized at 60 °C, 70 °C, 80 °C, 100 °C, and 120 °C was 6.148  $\mu\text{m}$ , 11.580  $\mu\text{m}$ , 11.829  $\mu\text{m}$ , 14.278  $\mu\text{m}$  and 22.932  $\mu\text{m}$ , respectively.
- (2) The kinetic process of chloride ion adsorption by CAL was more in line with the description of a Pseudo-second-order kinetic model and the Langmuir isotherm could fit the adsorption results of CAL samples better than the Freundlich isotherm. Theoretical maximum adsorption capacity of  $\text{Cl}^-$  on CAL prepared at 60–120 °C was 211.324 mg/g, 182.117 mg/g, 174.903 mg/g, 160.914 mg/g and 155.960 mg/g, respectively. Chloride uptake of CAL could be improved by increasing aging temperature due to particle size reduction.
- (3) The main adsorption mechanism of chloride ion on CAL was an interlayer anion exchange reaction other than the dissolution-precipitate mode. With increasing the pH of solution (7–13), chloride uptake of CAL increased slightly and a high pH level (11–12) was kept after adsorption. The presence of  $\text{CO}_3^{2-}$  and  $\text{SO}_4^{2-}$  with high concentration reduced the adsorption capacity of CAL significantly as compared with  $\text{OH}^-$  due to the destruction of layered structure and precipitates formed ( $\text{CaCO}_3$  or  $\text{CaSO}_4$ ). Interference sequence of three anions on the chloride uptake of CAL was  $\text{SO}_4^{2-} > \text{CO}_3^{2-} > \text{OH}^-$ , and the order of interlayer anionic affinity was  $\text{Cl}^- > \text{OH}^- > \text{NO}_3^-$ .
- (4) Although the results showed that the presence of  $\text{CO}_3^{2-}$  and  $\text{SO}_4^{2-}$  could affect the application of LDH in concrete, in actual conditions the concentration of  $\text{CO}_3^{2-}$  and  $\text{SO}_4^{2-}$  in concrete is low and the carbonation and sulfate attacks happen from the exterior surface of the concrete structure. So, it is believed incorporation of LDHs into concrete would still maintain its adsorption effect on  $\text{Cl}^-$ .

**Author Contributions:** Methodology, H.C. and S.Z.; experimental design and testing, F.Y., W.H. and D.Z.; data curation, W.H. and D.Z.; writing—original draft preparation, S.Z. and F.Y.; language modification, W.T.; writing—review and editing, H.C., L.L. and N.H.; funding acquisition, H.C. All authors have read and agreed to the published version of the manuscript.

**Funding:** The work described in this paper was fully supported by grants from Natural Science Foundation of China, grant number 51678366.

**Conflicts of Interest:** The authors declare no conflict of interest.

## References

1. Mehta, P.K.; Paulo, J.; Monteiro, M. *Concrete Microstructure, Properties and Materials*; McGraw-Hill Education: New York, NY, USA, 2017.
2. Tam, V.W.; Butera, A.; Le, K.N.; Li, W. Utilising CO<sub>2</sub> technologies for recycled aggregate concrete: A critical review. *Constr. Build. Mater.* **2020**, *250*, 118903. [[CrossRef](#)]
3. Sagoe-Crentsil, K.; Brown, T.; Taylor, A. Performance of concrete made with commercially produced coarse recycled concrete aggregate. *Cem. Concr. Res.* **2001**, *31*, 707–712. [[CrossRef](#)]
4. Pacheco, J.; De Brito, J.; Chastre, C.; Evangelista, L. Experimental investigation on the variability of the main mechanical properties of concrete produced with coarse recycled concrete aggregates. *Constr. Build. Mater.* **2019**, *201*, 110–120. [[CrossRef](#)]
5. Bao, J.; Li, S.; Zhang, P.; Ding, X.; Xue, S.; Cui, Y.; Zhao, T. Influence of the incorporation of recycled coarse aggregate on water absorption and chloride penetration into concrete. *Constr. Build. Mater.* **2020**, *239*, 117845. [[CrossRef](#)]
6. Quattrone, M.; Angulo, S.C.; John, V.M. Energy and CO<sub>2</sub> from high performance recycled aggregate production. *Resour. Conserv. Recycl.* **2014**, *90*, 21–33. [[CrossRef](#)]
7. Zhu, Y.-G.; Kou, S.-C.; Poon, C.-S.; Dai, J.-G.; Li, Q.-Y. Influence of silane-based water repellent on the durability properties of recycled aggregate concrete. *Cem. Concr. Compos.* **2013**, *35*, 32–38. [[CrossRef](#)]
8. Nandhini, K.; Ponmalar, V. Effect of Blending Micro and Nano Silica on the Mechanical and Durability Properties of Self-Compacting Concrete. *Silicon* **2020**, 1–9. [[CrossRef](#)]
9. García, R.; Reyes, E.; Villanueva, P.; De La Rubia, M.Á.; Fernández, J.; Moragues, A. Service Life and Early Age Durability Enhancement due to Combined Metakaolin and Nanosilica in Mortars for Marine Applications. *Materials (Basel)* **2020**, *13*, 1169. [[CrossRef](#)]
10. Prakasam, G.; Murthy, A.R.; Reheman, M.M.S.; Ganesh, P. Mechanical, Durability and Fracture Properties of Nano Modified FA-GGBS Geopolymer Mortar. *Mag. Concr. Res.* **2020**, *72*, 207–216. [[CrossRef](#)]
11. Yang, Z.; Sui, S.; Wang, L.; Feng, T.; Gao, Y.; Mu, S.; Tang, L.; Jiang, J. Improving the chloride binding capacity of cement paste by adding nano-Al<sub>2</sub>O<sub>3</sub>: The cases of blended cement pastes. *Constr. Build. Mater.* **2020**, *232*. [[CrossRef](#)]
12. Lv, S.; Hu, H.; Zhang, J.; Lei, Y.; Sun, L.; Hou, Y. Structure, performances, and formation mechanism of cement composites with large-scale regular microstructure by distributing uniformly few-layered graphene oxide in cement matrix. *Struct. Concr.* **2018**, *20*, 471–482. [[CrossRef](#)]
13. Li, G.; Zhou, J.; Yue, J.; Gao, X.; Wang, K. Effects of nano-SiO<sub>2</sub> and secondary water curing on the carbonation and chloride resistance of autoclaved concrete. *Constr. Build. Mater.* **2020**, *235*, 117465. [[CrossRef](#)]
14. Duan, P.; Chen, W.; Ma, J.; Shui, Z. Influence of layered double hydroxides on microstructure and carbonation resistance of sulphoaluminate cement concrete. *Constr. Build. Mater.* **2013**, *48*, 601–609. [[CrossRef](#)]
15. Yuan, Q.; Shi, C.; De Schutter, G.; Audenaert, K.; Deng, D. Chloride Binding of Cement-Based Materials Subjected to External Chloride Environment—A Review. *Constr. Build. Mater.* **2009**, *23*, 1–13. [[CrossRef](#)]
16. Chi, L.; Wang, Z.; Zhou, Y.; Lu, S.; Yao, Y. Layered Double Hydroxides Precursor as Chloride Inhibitor: Synthesis, Characterization, Assessment of Chloride Adsorption Performance. *Materials (Basel)* **2018**, *11*, 2537. [[CrossRef](#)] [[PubMed](#)]
17. Chen, Y.; Shui, Z.; Chen, W.; Chen, G. Chloride binding of synthetic Ca–Al–NO<sub>3</sub> LDHs in hardened cement paste. *Constr. Build. Mater.* **2015**, *93*, 1051–1058. [[CrossRef](#)]
18. Chung, C.-W.; Jung, H.-Y.; Kwon, J.-H.; Jang, B.-K.; Kim, J.-H. Use of calcium aluminum–layered double hydroxide to control chloride ion penetration of cement-based materials. *J. Struct. Integr. Maint.* **2019**, *4*, 37–42. [[CrossRef](#)]

19. Qu, Z.; Yu, Q.; Brouwers, H. Relationship between the particle size and dosage of LDHs and concrete resistance against chloride ingress. *Cem. Concr. Res.* **2018**, *105*, 81–90. [[CrossRef](#)]
20. Rojas, R. Copper, lead and cadmium removal by Ca Al layered double hydroxides. *Appl. Clay Sci.* **2014**, *87*, 254–259. [[CrossRef](#)]
21. Xu, S.; Zhang, B.; Chen, Z.; Yu, J.; Evans, D.G.; Zhang, F. A General and Scalable Formulation of Pure CaAl-Layered Double Hydroxide via an Organic/Water Solution Route. *Ind. Eng. Chem. Res.* **2011**, *50*, 6567–6572. [[CrossRef](#)]
22. Sipos, P.; Pálincó, I. As-prepared and intercalated layered double hydroxides of the hydrocalumite type as efficient catalysts in various reactions. *Catal. Today* **2018**, *306*, 32–41. [[CrossRef](#)]
23. Yang, Z.; Fischer, H.; Polder, R. Synthesis and characterization of modified hydrotalcites and their ion exchange characteristics in chloride-rich simulated concrete pore solution. *Cem. Concr. Compos.* **2014**, *47*, 87–93. [[CrossRef](#)]
24. Grover, K.; Komarneni, S.; Katsuki, H. Synthetic hydrotalcite-type and hydrocalumite-type layered double hydroxides for arsenate uptake. *Appl. Clay Sci.* **2010**, *48*, 631–637. [[CrossRef](#)]
25. Oladoja, N.; Adelagun, R.; Ololade, I.; Anthony, E.; Alfred, M. Synthesis of nano-sized hydrocalumite from a Gastropod shell for aqua system phosphate removal. *Sep. Purif. Technol.* **2014**, *124*, 186–194. [[CrossRef](#)]
26. Zhang, P.; Wang, T.; Zhang, L.; Wu, D.; Frost, R.L. XRD, SEM and infrared study into the intercalation of sodium hexadecyl sulfate (SHS) into hydrocalumite. *Spectrochim. Acta Part A Mol. Biomol. Spectrosc.* **2015**, *151*, 673–678. [[CrossRef](#)]
27. Milagres, J.L.; Bellato, C.R.; Vieira, R.S.; Ferreira, S.O.; Reis, C. Preparation and evaluation of the Ca-Al layered double hydroxide for removal of copper(II), nickel(II), zinc(II), chromium(VI) and phosphate from aqueous solutions. *J. Environ. Chem. Eng.* **2017**, *5*, 5469–5480. [[CrossRef](#)]
28. Li, Y.; Wang, J.; Li, Z.; Liu, Q.; Liu, J.; Liu, L.; Zhang, X.; Yu, J. Ultrasound assisted synthesis of Ca–Al hydrotalcite for U (VI) and Cr (VI) adsorption. *Chem. Eng. J.* **2013**, *218*, 295–302. [[CrossRef](#)]
29. Tathod, A.P.; Gazit, O.M. Fundamental Insights into the Nucleation and Growth of Mg–Al Layered Double Hydroxides Nanoparticles at Low Temperature. *Cryst. Growth Des.* **2016**, *16*, 6709–6713. [[CrossRef](#)]
30. Galvão, T.L.P.; Neves, C.; Caetano, A.P.; Maia, F.; Mata, D.; Malheiro, E.; Ferreira, M.J.; Bastos, A.; Salak, A.N.; Gomes, J.R.B.; et al. Control of crystallite and particle size in the synthesis of layered double hydroxides: Macromolecular insights and a complementary modeling tool. *J. Colloid Interface Sci.* **2016**, *468*, 86–94. [[CrossRef](#)]
31. Ji, H.; Wu, W.; Li, F.; Yu, X.; Fu, J.; Jia, L. Enhanced adsorption of bromate from aqueous solutions on ordered mesoporous Mg–Al layered double hydroxides (LDHs). *J. Hazard. Mater.* **2017**, *334*, 212–222. [[CrossRef](#)]
32. Wang, T.; Li, C.; Wang, C.; Wang, H. Biochar/MnAl-Ldh Composites for Cu (II) Removal from Aqueous Solution. *Colloids Surf. A Physicochem. Eng. Asp.* **2018**, *538*, 443–450.
33. Zhou, H.; Jiang, Z.; Wei, S. A New Hydrotalcite-Like Absorbent Femnmg-Ldh and Its Adsorption Capacity for Pb 2+ Ions in Water. *Appl. Clay Sci.* **2018**, *153*, 29–37.
34. Hatami, H.; Fotovat, A.; Halajnia, A. Comparison of adsorption and desorption of phosphate on synthesized Zn-Al LDH by two methods in a simulated soil solution. *Appl. Clay Sci.* **2018**, *152*, 333–341. [[CrossRef](#)]
35. Tamaki, T.; Nakanishi, N.; Ohashi, H.; Yamaguchi, T. The effect of particle size and surface area on the ion conductivity of layered double hydroxide. *Electrochem. Commun.* **2012**, *25*, 50–53. [[CrossRef](#)]
36. Kuroda, Y.; Miyamoto, Y.; Hibino, M.; Yamaguchi, K.; Mizuno, N. Tripodal Ligand-Stabilized Layered Double Hydroxide Nanoparticles with Highly Exchangeable CO<sub>3</sub><sup>2-</sup>. *Chem. Mater.* **2013**, *25*, 2291–2296. [[CrossRef](#)]
37. Zhang, P.G.; Qian, Z.P.; Xu, H.; Shi, X.; Ruan, J.; Yang, R.L. Effective Adsorption of Sodium Dodecylsulfate (Sds) by Hydrocalumite (CaAl-Ldh-Cl) Induced by Self-Dissolution and Re-Precipitation Mechanism. *J. Colloid. Interface Sci.* **2012**, *367*, 264–271. [[CrossRef](#)]
38. Qian, G.; Feng, L.; Zhou, J.; Xu, Y.; Liu, J.; Zhang, J.; Xu, Z.P. Solubility product (K<sub>sp</sub>)-controlled removal of chromate and phosphate by hydrocalumite. *Chem. Eng. J.* **2012**, *181*, 251–258. [[CrossRef](#)]
39. Dadwhal, M.; Sahimi, M.; Tsotsis, T.T. Adsorption Isotherms of Arsenic on Conditioned Layered Double Hydroxides in the Presence of Various Competing Ions. *Ind. Eng. Chem. Res.* **2011**, *50*, 2220–2226. [[CrossRef](#)]

